IEEE Access
Multidisciplinary | Rapid Review | Open Access Journal

Received March 2, 2019, accepted March 18, 2019, date of publication March 20, 2019, date of current version April 5, 2019.

Digital Object Identifier 10.1109/ACCESS.2019.2906551

A Tunable Balanced Coupler With Improved Phase Balance and Extended Bandwidth

PEI-LING CHI, (Senior Member, IEEE), HONG-MIN LIN, AND CHUN-PIN CHIEN
Department of Electrical and Computer Engineering, National Chiao Tung University, Hsinchu 300, Taiwan

Corresponding author: Pei-Ling Chi (peilingchi@nctu.edu.tw)

This work was supported by the Ministry of Science and Technology of Taiwan under Grant MOST 106-2221-E-009-018 and Grant MOST 107-2221-E-009-053.

ABSTRACT This paper proposes a balanced coupler with improved phase balance and extended bandwidth for a wide range of tunable power-dividing ratios. This differential coupler uses only two varactors and can demonstrate tunable power-dividing ratio and quadrature phase difference between outputs with theoretically perfect differential-mode return loss and port isolation, and complete common-mode suppression. The coupler analysis, design equations/graph, and parametric study will be given in detail. As a proof-of-concept, a microstrip prototype operating at 1 GHz was fabricated. Measured results show that the power-dividing ratio can be tuned from -5.5 dB to 11.9 dB at the center frequency where the insertion loss is less than 0.84 dB, the phase imbalance and isolation between differential outputs are less than 3.9° and greater than 23.2 dB, respectively. Moreover, the differential-mode return loss and the common-mode rejection are greater than 27.5 dB and 35.2 dB, respectively. Measured and simulated results are in good agreement.

INDEX TERMS Balanced, CMRR, differential, mixed-mode, power-dividing ratio, quadrature coupler, tunable, varactor.

I. INTRODUCTION

Balanced circuit architecture is known for featuring high immunity to various noise sources, such as those from adjacent circuitry, power supplies, and other external sources that are coupled electrically or electromagnetically and become notably influential in high-speed applications and/or highly-integrated products. As a result, the demands of stand-alone balanced/differential components have increased rapidly to improve communication performance and to reduce system size/loss due to the utilization of additional balun transformers between balanced and single-ended topologies. To this end, the designs of the balanced filters [1]–[6], diplexer [7], crossover [8], power dividers [9]–[19], and couplers [20]–[22] were extensively carried out. Particularly, the balanced power divider or coupler with arbitrary power-dividing ratios [12], [22], with filtering response [13], [19]–[21], or with scalable number of power outputs [17] was developed to enhance functional capabilities of the balanced circuit.

Over the past few years, to adapt to multi-standard communications, several balanced bandpass filters with frequency agility were reported [23]–[27], and the bandwidth control [25] or dual tunable passbands [27] was also attained therein. To enhance adaptability to dynamic communication environments, such as in smart antennas and software defined radios, the balanced power divider [28] or coupler [29] with tunable power-dividing ratio was recently reported. The power divider in [28] can achieve a wide tuning range at the center frequency. However, when low bias voltages are applied (corresponding to large varactor capacitances), the measured output phase imbalance ($\angle S_{AB}^{dd} - \angle S_{AC}^{dd}$) is up to 10° and thus may be inappropriate for practical applications. Similarly, the balanced coupler [29] in the absence of the active capacitance circuit shows significant phase imbalance. Moreover, it has narrow bandwidth, thus necessitating further bandwidth improvement. It is noted that, despite the great interest in the development of tunable single-ended couplers [30]–[31], a well-performed balanced coupler with a wide range of tunable power-dividing ratios is less reported thus far.

In this paper, a simple varactor-tuned balanced coupler structure is proposed. Specifically, the coupler's power-dividing ratio is tuned by a single control voltage across the shunt varactors and depending on the available capacitance tuning ratio, it can vary over a wide range. Furthermore, at all

The associate editor coordinating the review of this manuscript and approving it for publication was Wenjie Feng.

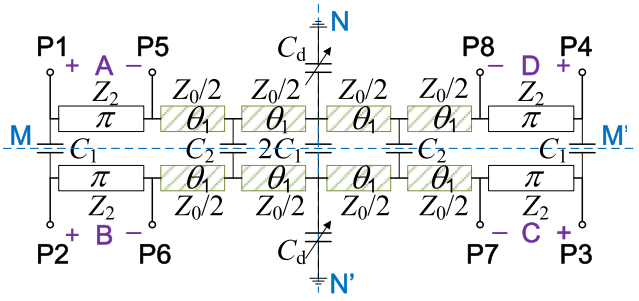

FIGURE 1. Configuration of proposed balanced quadrature coupler with tunable power-dividing ratio.

tuning states of the differential-mode operation, the proposed coupler can theoretically achieve perfect return loss and port isolation, and quadrature phase outputs. To derive governing equations, the mixed-mode S-parameters, the conversion techniques between the mixed-mode and standard S-parameters, as well as the even-odd mode analysis were used altogether. The closed-form formulas, design guidelines, and performance studies with respect to circuit parameters will be given in detail. For validation purposes, a microstrip prototype was developed with a measured tuning range from –5.5 dB to 11.9 dB, where the phase imbalance is less than 3.9° and the various differential-mode bandwidths are considerably expanded as compared to the existing tunable designs [28], [29].

II. ANALYSIS AND DESIGN OF PROPOSED BALANCED COUPLER WITH TUNABLE POWER-DIVIDING RATIO

A. ANALYSIS OF PROPOSED BALANCED COUPLER

The configuration of proposed balanced coupler with tunable power-dividing ratio is shown in Fig. 1. This coupler consists of eight transmission lines of characteristic impedance $0.5Z_0$ and of electrical length θ_1, four half-wavelength transmission lines of characteristic impedance Z_2, lumped capacitors of capacitances C_1 (or $2C_1$) and C_2, and two identical varactors of capacitance $C_{\rm d}$, which will be controlled by a single voltage $V_{\rm d}$. Note that the termination impedance of each port is Z_0 and it is 50 Ω here. The differential ports between ports 1 and 5, ports 2 and 6, ports 3 and 7, and ports 4 and 8 are defined as A, B, C, and D, respectively. Without loss of generality, if the differential port A is the input of the balanced coupler, ports B and C are outputs while port D is the isolated port. Thus, the power-dividing ratio k^2 is defined as follows:

$$k^2 = \left| \frac{S^{dd}_{CA}}{S^{dd}_{BA}} \right|^2. \tag{1}$$

It will be shown later that, by simply controlling the voltage across the shunt diodes, the power-dividing ratio of the coupler can be continuously tuned.

To realize ideal impedance matching and port isolation for differential-mode operation, no cross-mode conversion, and complete common-mode rejection, the mixed-mode scattering matrix (S^{mm}) of the coupler is of the form

$$S^{mm} = \begin{bmatrix} S^{dd} & S^{dc} \\ S^{cd} & S^{cc} \end{bmatrix} = \begin{bmatrix} 0 & a & b & 0 & 0 & 0 & 0 & 0 \\ a & 0 & 0 & b & 0 & 0 & 0 & 0 \\ b & 0 & 0 & a & 0 & 0 & 0 & 0 \\ 0 & b & a & 0 & 0 & 0 & 0 & 0 \\ 0 & 0 & 0 & 0 & c & 0 & 0 & 0 \\ 0 & 0 & 0 & 0 & 0 & c & 0 & 0 \\ 0 & 0 & 0 & 0 & 0 & 0 & c & 0 \\ 0 & 0 & 0 & 0 & 0 & 0 & 0 & c \end{bmatrix}, \tag{2}$$

where the 4×4 sub-matrices S^{dd}, S^{dc}, S^{cd}, and S^{cc} are given as follows:

$$S^{dd} = \begin{bmatrix} 0 & a & b & 0 \\ a & 0 & 0 & b \\ b & 0 & 0 & a \\ 0 & b & a & 0 \end{bmatrix}, \quad S^{cc} = \begin{bmatrix} c & 0 & 0 & 0 \\ 0 & c & 0 & 0 \\ 0 & 0 & c & 0 \\ 0 & 0 & 0 & c \end{bmatrix} \tag{3a}$$

$$S^{dc} = S^{cd} = [0]_{4\times4}. \tag{3b}$$

The matrix entries a, b, and c are given by

$$a = \frac{1}{\sqrt{1+k^2}} e^{j\varphi_1}, \quad b = \frac{k}{\sqrt{1+k^2}} e^{j\varphi_2}, \; c = e^{j\varphi_3}, \tag{4}$$

where φ_1 and φ_2 are the differential-mode transmission phase shifts, and φ_3 is the phase shift due to common-mode reflection. The standard scattering matrix (S^{std}) of this eight-port coupler can be obtained from the mixed-mode scattering matrix by [32]

$$S^{std} = M^{-1} S^{mm} M, \tag{5}$$

where, according to the port numbering shown in Fig. 1, the transformation matrix M is given as

$$M = \frac{1}{\sqrt{2}} \begin{bmatrix} 1 & 0 & 0 & 0 & -1 & 0 & 0 & 0 \\ 0 & 1 & 0 & 0 & 0 & -1 & 0 & 0 \\ 0 & 0 & 1 & 0 & 0 & 0 & -1 & 0 \\ 0 & 0 & 0 & 1 & 0 & 0 & 0 & -1 \\ 1 & 0 & 0 & 0 & 1 & 0 & 0 & 0 \\ 0 & 1 & 0 & 0 & 0 & 1 & 0 & 0 \\ 0 & 0 & 1 & 0 & 0 & 0 & 1 & 0 \\ 0 & 0 & 0 & 1 & 0 & 0 & 0 & 1 \end{bmatrix}. \tag{6}$$

Thus, the standard scattering matrix S^{std} can be readily obtained with (2), (5) and (6):

$$S^{std} = \frac{1}{2} \begin{bmatrix} c & a & b & 0 & c & -a & -b & 0 \\ a & c & 0 & b & -a & c & 0 & -b \\ b & 0 & c & a & -b & 0 & c & -a \\ 0 & b & a & c & 0 & -b & -a & c \\ c & -a & -b & 0 & c & a & b & 0 \\ -a & c & 0 & -b & a & c & 0 & b \\ -b & 0 & c & -a & b & 0 & c & a \\ 0 & -b & -a & c & 0 & b & a & c \end{bmatrix}. \tag{7}$$

Given the ideal scattering matrix in (7), the design equations of proposed balanced coupler can thereafter be derived.

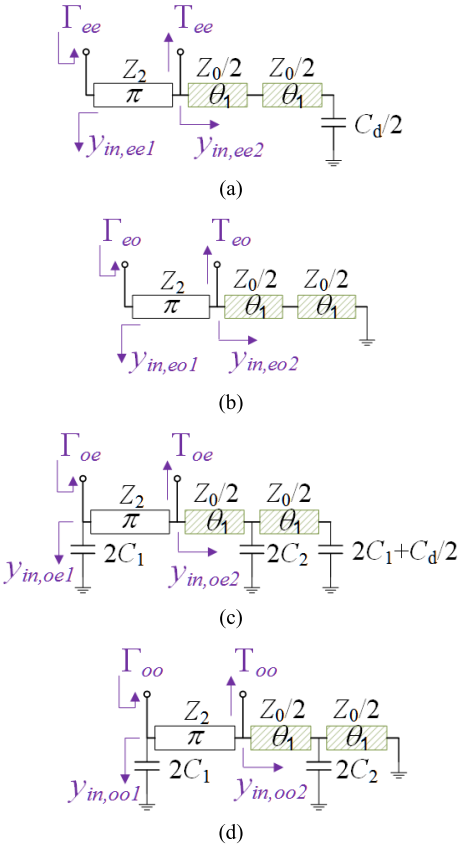

FIGURE 2. Four quarter circuits of proposed balanced quadrature coupler with tunable power-dividing ratio. (a) Open- and open-circuited, (b) open- and short-circuited, (c) short- and open-circuited, and (d) short- and short-circuited boundary conditions along the MM' and NN' planes, respectively.

As shown in Fig. 1, this coupler has twofold symmetry across the symmetric planes MM' and NN' and thus it can be analyzed by the even-odd mode analysis. By applying the open- or short-circuited boundary condition along each symmetric plane, the coupler can be decomposed into four quarter circuits, as shown in Fig. 2. Thus, the standard S-parameters of the balanced coupler can be reconstructed as

$$S_{11} = \frac{1}{4}(\Gamma_{ee} + \Gamma_{eo} + \Gamma_{oe} + \Gamma_{oo}) = \frac{c}{2} \tag{8a}$$

$$S_{51} = \frac{1}{4}(T_{ee} + T_{eo} + T_{oe} + T_{oo}) = \frac{c}{2} \tag{8b}$$

$$S_{21} = \frac{1}{4}(\Gamma_{ee} + \Gamma_{eo} - \Gamma_{oe} - \Gamma_{oo}) = \frac{a}{2} \tag{8c}$$

$$S_{61} = \frac{1}{4}(T_{ee} + T_{eo} - T_{oe} - T_{oo}) = \frac{-a}{2} \tag{8d}$$

$$S_{31} = \frac{1}{4}(\Gamma_{ee} - \Gamma_{eo} - \Gamma_{oe} + \Gamma_{oo}) = \frac{b}{2} \tag{8e}$$

$$S_{71} = \frac{1}{4}(T_{ee} - T_{eo} - T_{oe} + T_{oo}) = \frac{-b}{2} \tag{8f}$$

$$S_{41} = \frac{1}{4}(\Gamma_{ee} - \Gamma_{eo} + \Gamma_{oe} - \Gamma_{oo}) = 0 \tag{8g}$$

$$S_{81} = \frac{1}{4}(T_{ee} - T_{eo} + T_{oe} - T_{oo}) = 0. \tag{8h}$$

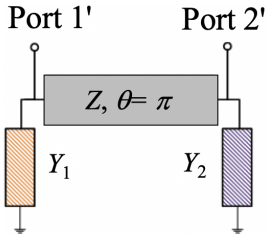

FIGURE 3. Two-port network containing a half-wavelength transmission line and two shunt admittances Y_1 and Y_2 on either side of the line.

where Γ_{ij} and T_{ij} ($i, j = e$ or o) represent, respectively, the reflection and transmission coefficients of each two-port quarter circuit and they are correlated. Note that every quarter circuit is in the form of the network shown in Fig. 3 where two ports are separated by a half-wavelength transmission line and two shunt admittances of Y_1 and Y_2 are loaded on either side of the line. It can be verified that the S-parameters of such a two-port network satisfy

$$S_{1'1'} + S_{2'1'} = -1, S_{1'2'} + S_{2'2'} = -1. \tag{9}$$

Thus, with (9), (8a) and (8b) lead to

$$S_{11} = \frac{1}{4}(\Gamma_{ee} + \Gamma_{eo} + \Gamma_{oe} + \Gamma_{oo}) = \frac{-1}{2}. \tag{10}$$

From (8g) and (10), the following relations yield

$$\Gamma_{ee} + \Gamma_{oe} = -1, \Gamma_{eo} + \Gamma_{oo} = -1. \tag{11}$$

In terms of the associated shunt admittances $y_{in,ij1}$ and $y_{in,ij2}$, the reflection coefficient Γ_{ij} of each quarter circuit can be derived from Fig. 2

$$\Gamma_{ij} = \frac{1 - Z_0 y_{in,ij}}{1 + Z_0 y_{in,ij}} = \frac{-Z_0(y_{in,ij1} + y_{in,ij2})}{2 + Z_0(y_{in,ij1} + y_{in,ij2})}, \tag{12}$$

where $y_{in,ij}$ is the corresponding input admittance for each Γ_{ij}. With (12), (11) can be expressed as follows:

$$(y_{in,ee1} + y_{in,ee2}) \cdot (y_{in,oe1} + y_{in,oe2}) = \left(\frac{2}{Z_0}\right)^2 \tag{13a}$$

$$(y_{in,eo1} + y_{in,eo2}) \cdot (y_{in,oo1} + y_{in,oo2}) = \left(\frac{2}{Z_0}\right)^2, \tag{13b}$$

where the shunt admittances are given as

$$y_{in,ee1} = 0, y_{in,ee2} = j\frac{2}{Z_0}\frac{\omega\frac{C_d}{2} + \frac{2}{Z_0}\tan 2\theta_1}{\frac{2}{Z_0} - \omega\frac{C_d}{2}\tan 2\theta_1} \tag{14a}$$

$$y_{in,eo1} = 0, y_{in,eo2} = -j\frac{2}{Z_0}\cot 2\theta_1 \tag{14b}$$

$$y_{in,oo1} = j\omega 2C_1, \tag{14c}$$

$$y_{in,oo2} = j\frac{2}{Z_0}\frac{\omega C_2 + \frac{1}{Z_0}(\tan\theta_1 - \cot\theta_1)}{\frac{2}{Z_0} - \omega C_2 \tan\theta_1}, \tag{14d}$$

and (14c) is shown at the top of the next page. From (13) and (14), it is noted that the characteristic impedance Z_2 of the half-wavelength transmission line is not involved and

$$y_{in,oe1} = j\omega 2C_1,$$
$$y_{in,oe2} = j\frac{2}{Z_0}\frac{\frac{2}{Z_0}\omega\left(2C_1+\frac{C_d}{2}\right)+\frac{8}{Z_0^2}\tan\theta_1+\frac{4}{Z_0}\omega C_2-\frac{2}{Z_0}\omega\left(2C_1+\frac{C_d}{2}\right)\tan^2(\theta_1)-2C_2\omega^2\tan\theta_1\left(2C_1+\frac{C_d}{2}\right)}{\left(\frac{2}{Z_0}\right)^2-\frac{4}{Z_0}\omega\left(2C_1+\frac{C_d}{2}\right)\tan\theta_1-\frac{4}{Z_0}\omega C_2\tan\theta_1+2\omega^2C_2\left(2C_1+\frac{C_d}{2}\right)\tan^2(\theta_1)-\left(\frac{2}{Z_0}\right)^2\tan^2(\theta_1)} \quad (14c)$$

thus it can be favorably chosen to enhance the coupler performance. Detailed examination of the effect of this characteristic impedance will be given in Section II-B. By substituting the admittances in (14) into (13) and after some mathematical manipulations, two sets of solutions for capacitances C_1 and C_2 can be solved as

$$C_1 = \frac{1}{\omega Z_0}\left(\frac{\csc\theta_1}{\sin\theta_1+\cos\theta_1}\right),$$
$$C_2 = \frac{1}{\omega Z_0}\left(1+2\cot\theta_1-\cot^2\theta_1\right), \quad (15)$$
$$C_1 = \frac{1}{\omega Z_0}\left(\frac{\csc\theta_1}{\cos\theta_1-\sin\theta_1}\right),$$
$$C_2 = \frac{1}{\omega Z_0}\left(-1+2\cot\theta_1+\cot^2\theta_1\right). \quad (16)$$

Thus, the (fixed) capacitances C_1 and C_2 can be decided according to (15) and (16) for a given θ_1 and the operating (angular) frequency ω. Note that, to avoid the self-resonance effects of lumped capacitors, the capacitance values derived from (15), which are on the order of several picofarads, are used for coupler design and the calculated results for $\theta_1 \leq 90°$ are illustrated in Fig. 4. The operating frequency is 1 GHz

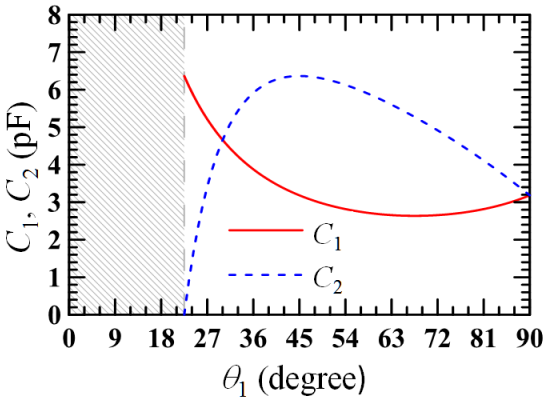

FIGURE 4. Calculated capacitances C_1 and C_2 with respect to θ_1 ($0° \leq \theta_1 \leq 90°$).

and for the purpose of size reduction, the electrical length θ_1 is limited within a quarter wavelength. Note that the gray area represent the unusable region where $C_2 < 0$ and thus the applicable electrical length is $22.5° \leq \theta_1 \leq 90°$. Similar to the case for Z_2, proper determination of the value θ_1 through a parametric study will be discussed in Section II-B. From the above analysis, it is noted that the varactor capacitance C_d will not affect the differential-mode operation or common-mode suppression at the center frequency. On the other hand, the capacitance C_d is related to the power-dividing ratio k^2. The power-dividing ratio k^2 of the proposed balanced coupler is given as

$$k^2 = \left|\frac{S_{CA}^{dd}}{S_{BA}^{dd}}\right|^2 = \left|\frac{S_{31}}{S_{21}}\right|^2 = \left|\frac{\Gamma_{ee}-\Gamma_{eo}-\Gamma_{oe}+\Gamma_{oo}}{\Gamma_{ee}+\Gamma_{eo}-\Gamma_{oe}-\Gamma_{oo}}\right|^2, \quad (17)$$

where, with (11), (14a) and (14b), the ratio k^2 can be further simplified as follows:

$$k^2 = \left|\frac{j4}{\omega Z_0 C_d}\right|^2. \quad (18)$$

Thus, the power-dividing ratio of this coupler can be simply controlled by the varactor capacitance C_d, which facilitates the implementation of tunable power-dividing ratio. In other words, given a power-dividing ratio k^2, the required C_d can be decided. Besides, it is seen that, ideally, the differential outputs are quadrature in phase and the proposed balanced coupler is therefore a quadrature coupler. As long as the capacitance values in (15) are satisfied, the ideal differential-mode return loss, isolation, quadrature phase outputs, and common-mode suppression can be theoretically maintained when the balanced coupler is tuned by the tuning capacitance C_d to realize a continuously varied power-dividing ratio.

B. DISCUSSIONS, PARAMETRIC STUDIES, AND DESIGN EXAMPLES

The design equation (18) shows that the varactor capacitance C_d decreases as the power ratio k^2 increases. The proposed coupler structure can enable a wide range of power-dividing ratios, including negative ($|S_{BA}^{dd}| > |S_{CA}^{dd}|$), zero (equal division), and positive ($|S_{BA}^{dd}| < |S_{CA}^{dd}|$) values in dB. Moreover, as C_d approaches 0, nearly all the input power is distributed to the differential port C, leading to the crossover response. On the other hand, the capacitances C_1 and C_2 are functions of θ_1 and are determined as soon as θ_1 is given. As aforementioned, by a proper choice of θ_1 and Z_2, the design can yield improved performance. Fig. 5 shows the simulated results of the coupler's fractional bandwidths against Z_2 when θ_1 is 27°, 40.5°, 54°, 67.5°, or 81°. The simulation was performed in the Advanced Design System (ADS) and, for comparison purposes only, the coupler was developed with ideal/lossless transmission lines and lumped elements. The calculated bandwidth, defined in terms of the differential-mode return loss, the output magnitude imbalance (< 0.5 dB), or the output phase imbalance (< 5°), is shown in Fig. 5 (a), (b), or (c), respectively. Those results are derived from the power-dividing ratio of 0 dB, which requires the capacitance C_d of 12.7 pF. Note that due to the wide applicability of a

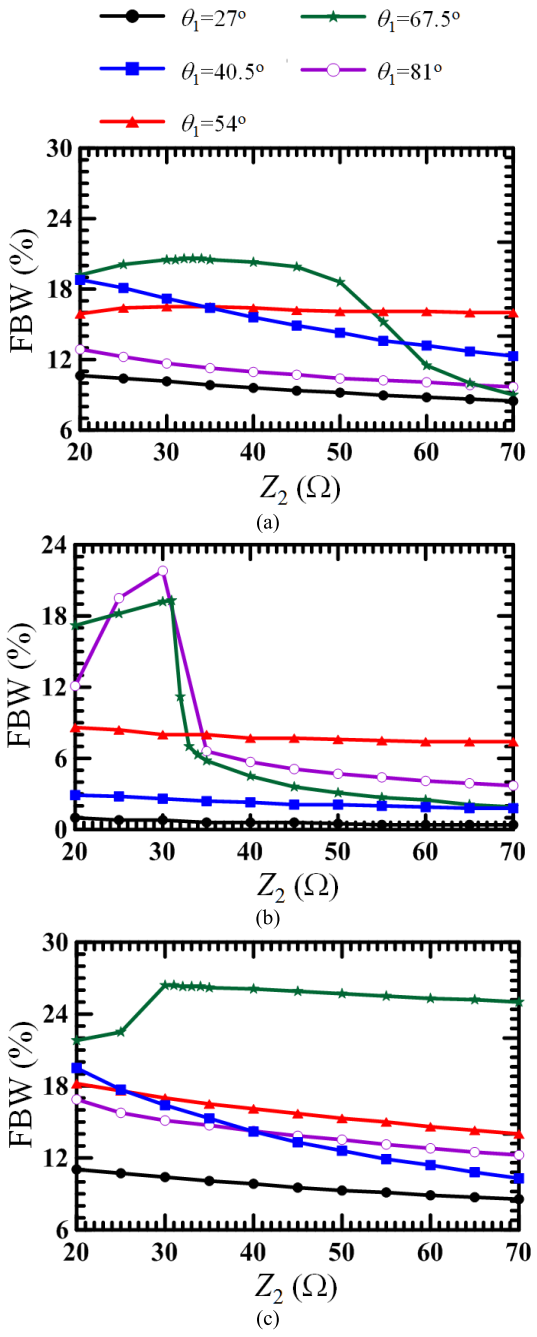

FIGURE 5. Circuit-simulated fractional bandwidths (FBWs) of proposed balanced coupler. The center frequency and the power-dividing ratio are 1 GHz and 0 dB, respectively. (a) For $\left|S_{AA}^{dd}\right| < -15$ dB, (b) for $||S_{CA}^{dd}| - |S_{BA}^{dd}|| < 0.5$ dB, and (c) for $\left|\angle S_{CA}^{dd} - \angle S_{BA}^{dd} - 90°\right| < 5°$.

hybrid coupler (equal power-split), the determination of θ_1 and Z_2 essentially depends on the case examination of 0 dB. To improve the bandwidths at any particular power ratio, the bandwidth study for that power ratio can be conducted to find proper values. It is seen that the parameter θ_1 has substantial effects on the attainable fractional bandwidths. Specifically, the case of $\theta_1 = 67.5°$ exhibits superior bandwidth performance and thus will be used for coupler development. On the other hand, low characteristic impedance Z_2 will contribute to a somewhat increased bandwidth. Note that, as the impedance Z_2 varies from 20 Ω to 30 Ω in the case of θ_1 =67.5° or 81° in Fig. 5 (b), the insertion-loss curves (S_{BA}^{dd}, S_{CA}^{dd}) follow each other closely with less than 0.5-dB difference at the low-frequency side and thus yields an increased bandwidth.

To validate the applicability of given design equations for the proposed structure, the balanced coupler was developed in ADS for the power-dividing ratios of -6 dB, -3 dB, 0 dB, 3 dB, 6 dB, and 10 dB. For demonstration purposes, the coupler was again designed with lossless transmission lines and lumped elements. In this design, the parameters θ_1, Z_2, C_1, and C_2 are 67.5°, 30 Ω, 2.64 pF, and 5.27 pF, respectively. The simulated mixed-mode S-parameters are shown in Figs. 6 and 7. The required value C_d for each power-dividing ratio is indicated in Fig. 6 (a). In differential mode, the coupler achieves perfect return loss $|S_{AA}^{dd}|$ and port isolation $|S_{DA}^{dd}|$, and maintains quadrature phase difference at the center frequency for all states. To improve clarity, Fig. 7 depicts only two cases where the full common-mode suppression and no differential- to common-mode conversion (or vice versa) are observed at the center frequency.

The design procedure of proposed balanced quadrature coupler is summarized as follows.

Step 1) Proper determination of the parameters θ_1 and Z_2. The bandwidth studies shown in Fig. 5 can be referenced, and if necessary, similar studies at other power-dividing ratios can be conducted. Moreover, the length/size reduction and fabrication convenience are other practical factors for choice of θ_1 and Z_2.

Step 2) Use (15) or Fig. 4 (for the center frequency at 1 GHz) to obtain the corresponding capacitances C_1 and C_2 for a given θ_1 decided in Step 1).

Step 3) Use (18) to compute the required varactor capacitance C_d for each power-dividing ratio. The data sheet from the manufacturer of varactor diodes can then be used for initial determination of the required control voltage.

III. EXPERIMENTAL AND SIMULATED RESULTS

The proposed balanced quadrature coupler was developed at 1 GHz and fabricated on the RT/duroid 5880 substrate of thickness 0.508 mm and of dielectric constant 2.2. The photograph and physical layout are shown in Fig. 8. To carry out the variable capacitance C_d, the silicon varactor diode SMV1232 from Skyworks was used as the tuning element and controlled by a single voltage V_d. Based on the design guidelines in Section II-B, the electrical length θ_1 of 67.5° and the characteristic impedance Z_2 of 30 Ω were chosen and the corresponding (fixed) capacitances C_1 and C_2 were readily determined by (15). To reduce parasitic effects, in particular, the capacitance C_1 was realized by two Murata GQM1885C capacitors of 1.3 pF in parallel connection. Similarly, two Murata GRM1885C capacitors of 2.6 pF were connected in parallel to implement the capacitance C_2. Note that to avoid the effects of unwanted coupling, a sufficiently large gap (g =2 mm) between parallel lines was realized and at

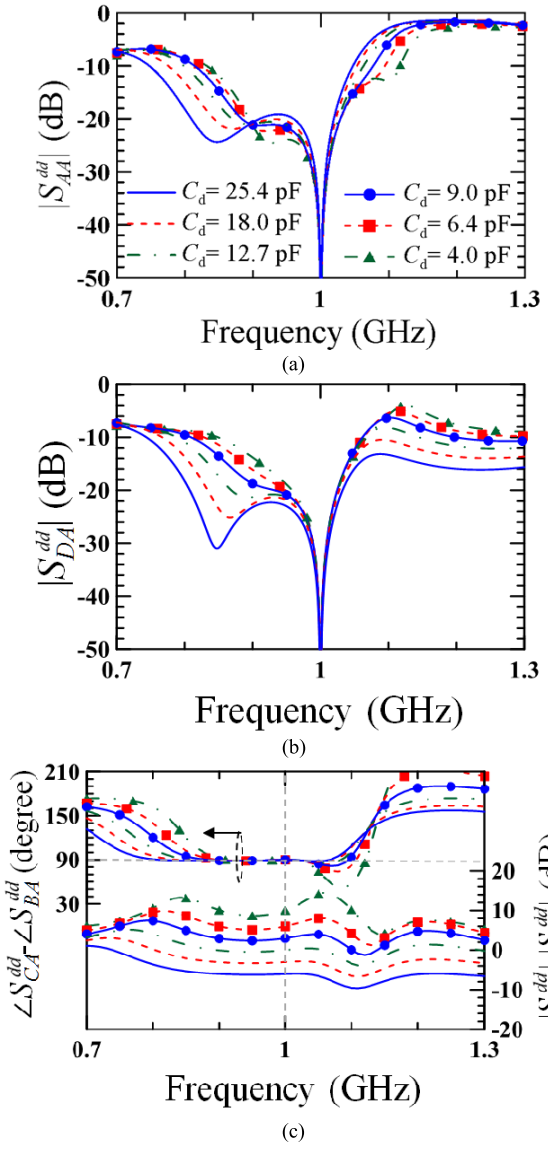

FIGURE 6. Circuit-simulated mixed-mode *S*-parameters. (a) $|S_{AA}^{dd}|$, (b) $|S_{DA}^{dd}|$, and (c) the phase difference $\angle S_{CA}^{dd} - \angle S_{BA}^{dd}$ and power-dividing ratio $|S_{CA}^{dd}| - |S_{BA}^{dd}|$.

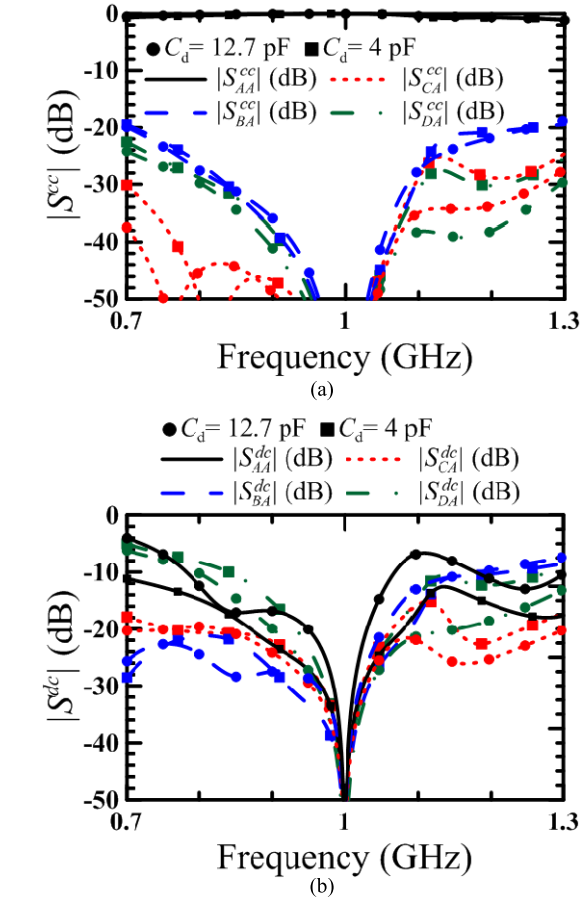

FIGURE 7. Circuit-simulated mixed-mode *S*-parameters. (a) $|S^{cc}|$ and (b) $|S^{dc}|$.

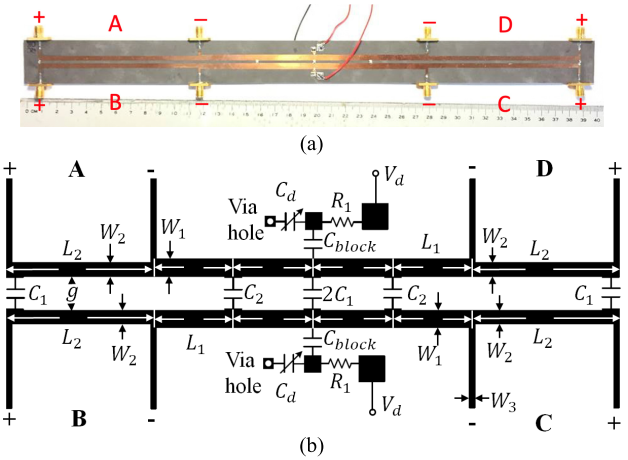

FIGURE 8. (a) Photograph and (b) the physical layout of fabricated balanced quadrature coupler with tunable power-dividing ratio.

the load position, a small extension of line width was used for mounting each lumped capacitor of package size 0603. Moreover, the DC block capacitance of 94 pF and the bias resistance of 1 MΩ were used. The proposed differential coupler was simulated by the electromagnetic solvers, Sonnet and ADS. To increase the prediction accuracy, the Sonnet and ADS are responsible for, respectively, the characterization of distributed line structures and lumped elements, such as the surface-mount varactors, capacitors, and bias resistors. The geometrical dimensions are denoted in Fig. 8 (b) and the values are given in Table 1.

Figs. 9 and 10 show measured and simulated mixed-mode *S*-parameters of the fabricated balanced quadrature coupler. Specifically, the power-dividing ratios of -5.5 dB and 0.21 dB are given here. It is seen that the experimental and simulated results are in good agreement. The bias voltage is indicated for each tuning state. When the control voltage increases, the varactor capacitance decreases and thus, according to (18), this will result in an increased power ratio, as obtained from the experimental results. Across the tuning range, the measured differential-mode return loss and port isolation are greater than 27.5 dB and 23.2 dB, respectively.

TABLE 1. Physical parameters of fabricated balanced coupler with tunable power-dividing ratio.

L_1 (mm)	W_1 (mm)	L_2 (mm)	W_2 (mm)
40	4	108.8	3.1
W_3 (mm)	g (mm)	d_{via} (mm)	
1.5	2	0.6	
C_1 (pF)	C_2 (pF)	C_{block} (pF)	R_1 (Ω)
2.6	5.2	94	1 M

d_{via}: diameter of the via hole.

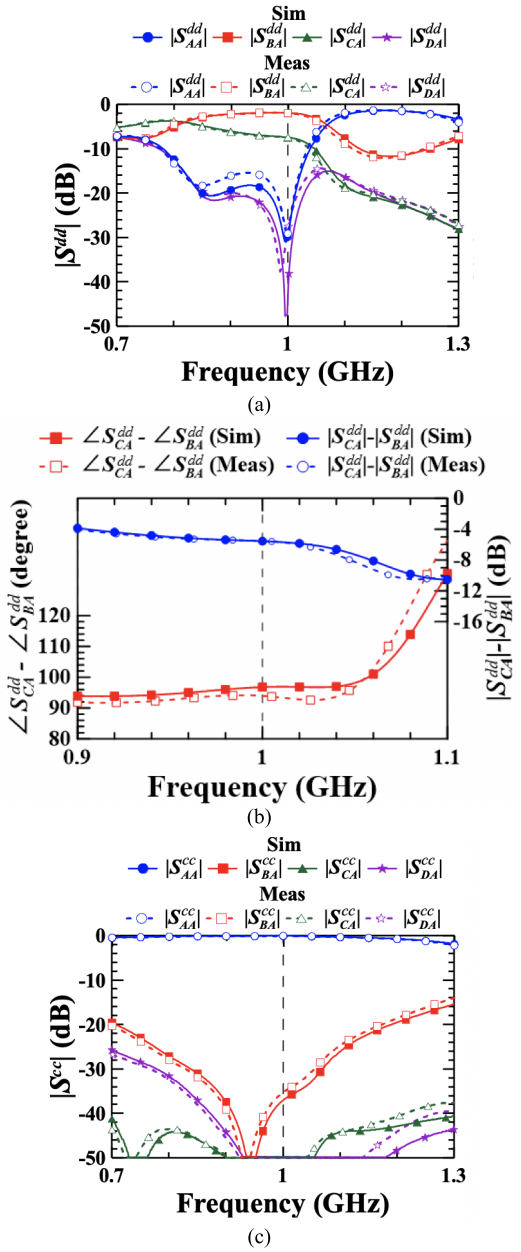

FIGURE 9. Measured and simulated results of proposed balanced quadrature coupler. The control voltage V_d = 0.4 V. The power-dividing ratio and phase difference between differential outputs are -5.5 dB and 93.9°, respectively. (a) $|S^{dd}|$, (b) $\angle S^{dd}_{CA} - \angle S^{dd}_{BA}$ and $|S^{dd}_{CA}| - |S^{dd}_{BA}|$, and (c) $|S^{cc}|$.

The measured insertion loss, defined as $|S^{dd}_{BA}|^2 + |S^{dd}_{CA}|^2$, attains its maximum of 0.84 dB and the minimum of 0.47 dB at the power ratios of -5.5 dB and 11.9 dB, respectively.

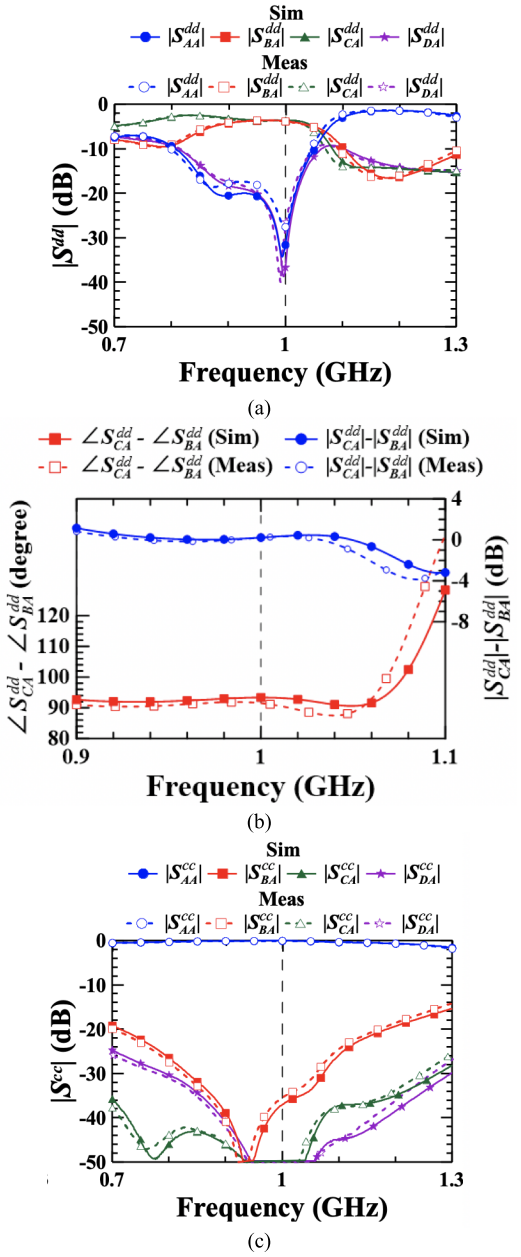

FIGURE 10. Measured and simulated results of proposed balanced quadrature coupler. The control voltage V_d = 1.7 V. The power-dividing ratio and phase difference between differential outputs are 0.21 dB and 91.5°, respectively. (a) $|S^{dd}|$, (b) $\angle S^{dd}_{CA} - \angle S^{dd}_{BA}$ and $|S^{dd}_{CA}| - |S^{dd}_{BA}|$, and (c) $|S^{cc}|$.

Note that the above-mentioned insertion loss includes the connector loss and the insertion loss is mainly attributed to the conductor and varactor losses. On the other hand, the common-mode suppression ($|S^{cc}_{BA}|$ or $|S^{cc}_{CA}|$) is greater than 35.2 dB at 1 GHz. Across the tuning range, the measured bandwidth is greater than 9.9% for the differential-mode return loss and port isolation of greater than 15 dB, and the phase imbalance of less than 3.9°. The 20-dB common-mode suppression exhibits a wide bandwidth of greater than 47.3%. For the phase imbalance less than 3.9°, the fabricated balanced coupler can experimentally realize a wide tuning

TABLE 2. Performance comparison of this work and prior balanced designs.

	Power-dividing ratio (PDR) (dB)	Phase imbalance @ f_0	Number of ports	Size ($\lambda_g \times \lambda_g$)	Differential-mode					BW (%) Common-mode suppression > 20 dB
					Insertion loss (dB) @ f_0	BW (%) Return loss > 15 dB	BW (%) Isolation > 15 dB	BW (%) Phase imbalance < 5°	BW (%) Magnitude imbalance < 0.5 dB	
This Work	-5.5 - 11.9 (tunable)	< 3.9°	8	1.85×0.079 (0.146 λ_g^2)	0.70 (PDR = 0)	> 17.6	> 9.9	> 11.5	13.4 (PDR=0)	> 47.3
[12]	9.38 (fixed)	~3°	6	0.5×0.75 (0.375 λ_g^2)	0.47	> 17	55	15	> ~43	> 33
[22]	0, 3, 6 (fixed)	< 5°	8	0.52×0.5 (0.26 λ_g^2)	0.45 (PDR = 0)	> 4.3	> 4.8	> 6.4	~5.5 (PDR=0)	> 24.3
[28]	-22.7 - 8.2 (tunable)	< 10°	6	0.4×0.2 (0.08 λ_g^2)	0.7 (PDR = 0)	> 6.3	> 41	×	~2.5 (PDR=0)	> 46
[29]	-11.3 - 10.2 (tunable)	< 25°	8	0.88×0.21 (0.185 λ_g^2)	1.2 (PDR = 0)	> 4.1	×	×	~0.6 (PDR=0)	> 20.5

BW: Bandwidth. Phase imbalance: $|\angle S_{CA}^{dd} - \angle S_{BA}^{dd} - 90^\circ|$. Magnitude imbalance: $\left||S_{CA}^{dd}| - |S_{BA}^{dd}| - PDR\right|$.

range of 17.4 dB, i.e., 11.9-(-5.5), in a continuous fashion. In Table 2, circuit performances of this balanced and tunable coupler is compared to the balanced couplers or power dividers that can demonstrate tunable power-dividing ratio [28], [29] or that are designed with arbitrary power division [12], [22]. In terms of the enhanced functionality, this proposed balanced coupler, the recently reported power divider [28] and coupler [29] enable tunable power-dividing ratio while the other two (or most balanced components in the literature) are designed with fixed applications. Compared to the tunable designs in [28] and [29], this presented tunable coupler is able to maintain output phase relation within a small imbalance (< 3.9°) whereas the phase imbalance up to 10° or 25° from the ideal value, as reported in [28] or [29], is typically impractical. For the bandwidth of power division within 0.5-dB imbalance, the proposed coupler format renders substantial bandwidth enhancement in comparison with the tunable power divider [28] and coupler [29]. Note that, although the given comparison in Table II is based on the results evaluated at equal power division (PDR=0), it can be shown that such bandwidth enhancement also applies to other power-dividing ratios when compared to the tunable coupler in [29]. Moreover, even though the proposed structure is an eight-port coupler, its footprint size is smaller than the balanced power divider (six ports) [12] and the balanced couplers (eight ports) [22], [29]. As a proof-of-concept, the proposed coupler was fabricated in its unfolded form where the electrical length θ_1 of 67.5° was chosen for bandwidth enhancement. If the available length is of primary concern, a smaller value of θ_1 can be used for each corresponding section.

IV. CONCLUSION

A microstrip balanced coupler with tunable power-dividing ratio is proposed, fabricated, and measured. By applying a single control voltage, the power-dividing ratio can be experimentally tuned from -5.5 dB to 11.9 dB with substantial reduction of phase imbalance and of frequency variation of a given power-dividing ratio, thus rendering considerable bandwidth extension, as compared to the state-of-the-art. The design equations and design principles are discussed in detail.

REFERENCES

[1] J. Shi and Q. Xue, "Balanced bandpass filters using center-loaded half-wavelength resonators," *IEEE Trans. Microw. Theory Techn.*, vol. 58, no. 4, pp. 970–977, Apr. 2010.

[2] J. Shi and Q. Xue, "Dual-band and wide-stopband single-band balanced bandpass filters with high selectivity and common-mode suppression," *IEEE Trans. Microw. Theory Techn.*, vol. 58, no. 8, pp. 2204–2212, Aug. 2010.

[3] Y.-H. Cho and S.-W. Yun, "Design of balanced dual-band bandpass filters using asymmetrical coupled lines," *IEEE Trans. Microw. Theory Techn.*, vol. 61, no. 8, pp. 2814–2820, Aug. 2013.

[4] A. Fernández-Prieto, A. Lujambio, J. Martel, F. Medina, F. Mesa, and R. R. Boix, "Simple and compact balanced bandpass filters based on magnetically coupled resonators," *IEEE Trans. Microw. Theory Techn.*, vol. 63, no. 6, pp. 1843–1853, Jun. 2015.

[5] L. Yang, W.-W. Choi, K.-W. Tam, and L. Zhu, "Balanced dual-band bandpass filter with multiple transmission zeros using doubly short-ended resonator coupled line," *IEEE Trans. Microw. Theory Techn.*, vol. 63, no. 7, pp. 2225–2232, Jul. 2015.

[6] F. Wei, P. Y. Qin, Y. J. Guo, C. Ding, and X. W. Shi, "Compact balanced dual- and tri-band BPFs based on coupled complementary split-ring resonators (C-CSRR)," *IEEE Microw. Wireless Compon. Lett.*, vol. 26, no. 2, pp. 107–109, Feb. 2016.

[7] Y. Zhou, H.-W. Wei, and Y. Zhao, "Compact balanced-to-balanced microstrip diplexer with high isolation and common-mode suppression," *IEEE Microw. Wireless Compon. Lett.*, vol. 24, no. 3, pp. 143–145, Mar. 2014.

[8] Y.-H. Pang, E. D. Lin, and Y.-Y. Chen, "A planar balanced crossover," *IEEE Trans. Microw. Theory Techn.*, vol. 64, no. 6, pp. 1812–1821, Jun. 2016.

[9] J. W. May and G. M. Rebeiz, "A 40-50-GHz SiGe 1: 8 differential power divider using shielded broadside-coupled striplines," *IEEE Trans. Microw. Theory Techn.*, vol. 56, no. 7, pp. 1575–1581, Jul. 2008.

[10] L.-S. Wu, B. Xia, W.-Y. Yin, and J. Mao, "A half-mode substrate integrated waveguide ring for two-way power division of balanced circuit," *IEEE Microw. Wireless Compon. Lett.*, vol. 22, no. 7, pp. 333–335, Jul. 2012.

[11] B. Xia, L.-S. Wu, and J.-F. Mao, "A new balanced-to-balanced power divider/combiner," *IEEE Trans. Microw. Theory Techn.*, vol. 60, no. 9, pp. 2791–2798, Sep. 2012.

[12] B. Xia, L.-S. Wu, S.-W. Ren, and J.-F. Mao, "A balanced-to-balanced power divider with arbitrary power division," *IEEE Trans. Microw. Theory Techn.*, vol. 61, no. 8, pp. 2831–2840, Aug. 2013.
[13] L.-S. Wu, Y.-X. Guo, and J.-F. Mao, "Balanced-to-balanced Gysel power divider with bandpass filtering response," *IEEE Trans. Microw. Theory Techn.*, vol. 61, no. 12, pp. 4052–4062, Dec. 2013.
[14] J. Shi, J. Wang, K. Xu, J.-X. Chen, and W. Liu, "A balanced-to-balanced power divider with wide bandwidth," *IEEE Microw. Wireless Compon. Lett.*, vol. 25, no. 9, pp. 573–575, Sep. 2015.
[15] W. Feng, C. Zhao, W. Che, and Q. Xue, "Wideband balanced network with high isolation using double-sided parallel-strip line," *IEEE Trans. Microw. Theory Techn.*, vol. 63, no. 12, pp. 4013–4018, Dec. 2015.
[16] W. Feng, C. Zhao, W. Che, and Q. Xue, "A balanced-to-balanced network with unequal power division and wideband common mode suppression," *IEEE Microw. Wireless Compon. Lett.*, vol. 26, no. 4, pp. 237–239, Apr. 2016.
[17] J. Shi, K. Xu, W. Zhang, J.-X. Chen, and G. Zhai, "An approach to 1-to- 2^n way microstrip balanced power divider," *IEEE Trans. Microw. Theory Techn.*, vol. 64, no. 12, pp. 4222–4231, Dec. 2016.
[18] S. Chen, W.-C. Lee, and T.-L. Wu, "A balanced-to-balanced power divider with common-mode noise absorption," in *IEEE MTT-S Int. Microw. Symp. Dig. (IMS)*, May 2016, pp. 1–4.
[19] Y.-T. Chiu, Y.-H. Pang, and H.-C. Huang, "Differential unequal power divider with bandpass response," in *Proc. ISAP*, Oct. 2016, pp. 900–901.
[20] J. Shi *et al.*, "A balanced filtering branch-line coupler," *IEEE Microw. Wireless Compon. Lett.*, vol. 26, no. 2, pp. 119–121, Feb. 2016.
[21] Y.-J. Huang and Y.-H. Pang, "Balanced-to-balanced rat-race coupler with bandpass response," in *Proc. ISAP*, Oct. 2016, pp. 902–903.
[22] J. Shi, J. Qiang, K. Xu, and J.-X. Chen, "A balanced branch-line coupler with arbitrary power division ratio," *IEEE Trans. Microw. Theory Techn.*, vol. 65, no. 1, pp. 78–85, Jan. 2017.
[23] Y. C. Li and Q. Xue, "Tunable balanced bandpass filter with constant bandwidth and high common-mode suppression," *IEEE Trans. Microw. Theory Techn.*, vol. 59, no. 10, pp. 2452–2460, Oct. 2011.
[24] J. Mao, W. Che, Y. Ma, and J. Chen, "Tunable differential-mode bandpass filters with wide tuning range and high common-mode suppression," *IET Microw. Antennas Propag.*, vol. 8, no. 6, pp. 437–444, Apr. 2014.
[25] H. Zhu and A. M. Abbosh, "Tunable balanced bandpass filter with wide tuning range of center frequency and bandwidth using compact coupled-line resonator," *IEEE Microw. Wireless Compon. Lett.*, vol. 26, no. 1, pp. 7–9, Jan. 2016.
[26] L.-H. Zhou, Y.-L. Ma, J. Shi, J.-X. Chen, and W. Q. Che, "Differential dual-band bandpass filter with tunable lower band using embedded DGS unit for common-mode suppression," *IEEE Trans. Microw. Theory Techn.*, vol. 64, no. 12, pp. 4183–4191, Dec. 2016.
[27] W. Jiang, T. Wang, Y. Peng, T. Xia, and G. Wang, "Design of balanced dual-band filter with reconfigurable center frequencies," in *IEEE MTT-S Int. Microw. Symp. Dig.*, Jun. 2017, pp. 929–932.
[28] Y. Xiao, F. Lin, H. Ma, X. Tan, and H. Sun, "A planar balanced power divider with tunable power-dividing ratio," *IEEE Trans. Microw. Theory Techn.*, vol. 65, no. 12, pp. 4871–4882, Dec. 2017.
[29] F. Lin, "A planar balanced quadrature coupler with tunable power-dividing ratio," *IEEE Trans. Ind. Electron.*, vol. 65, no. 8, pp. 6515–6526, Aug. 2018.
[30] M. Zhou, J. Shao, B. Arigong, H. Ren, R. Zhou, and H. Zhang, "A varactor based 90° directional coupler with tunable coupling ratios and reconfigurable responses," *IEEE Trans. Microw. Theory Techn.*, vol. 62, no. 3, pp. 416–421, Mar. 2014.
[31] P.-L. Chi and T.-C. Hsu, "Highly reconfigurable quadrature coupler with ideal impedance matching and port isolation," *IEEE Trans. Microw. Theory Techn.*, vol. 65, no. 8, pp. 2930–2941, Aug. 2017.
[32] D. E. Bockelman and W. R. Eisenstadt, "Combined differential and common-mode scattering parameters: Theory and simulation," *IEEE Trans. Microw. Theory Techn.*, vol. 43, no. 7, pp. 1530–1539, Jul. 1995.

PEI-LING CHI (S'08–M'11–SM'17) received the B.S. and M.S. degrees in communication engineering from National Chiao Tung University (NCTU), Hsinchu, Taiwan, in 2004 and 2006, respectively, and the Ph.D. degree in electrical engineering from the University of California at Los Angeles (UCLA), in 2011.

Since 2011, she has been with National Chiao Tung University, as an Assistant Professor of electrical and computer engineering, where she is currently an Associate Professor. She holds several U.S. and international patents in the area of the left-handed metamaterials and has co-authored over 60 journal and conference papers. Her research interests include the analysis and design of the left-handed metamaterial circuits, design of microwave/mm-wave components and integrated systems, and development of terahertz antennas and communications. She is an Associate Editor of the IEEE MICROWAVE AND WIRELESS COMPONENTS LETTERS.

Dr. Chi was a recipient of the Research Creativity Award from the National Science Council, Taiwan, in 2004.

HONG-MIN LIN received the B.S. degree in electrical engineering from the National Taiwan University of Science and Technology, Taipei, Taiwan, in 2015, and the M.S. degree from the Institute of Communications Engineering, National Chiao Tung University (NCTU), Hsinchu, Taiwan, in 2017.

He is currently a System Engineer with RealTek Inc., Hsinchu, Taiwan.

CHUN-PIN CHIEN received the B.S. degree in electronic engineering from Chang Gung University, Taoyuan, Taiwan, in 2017. He is currently pursuing the M.S. degree with the Institute of Communications Engineering, National Chiao Tung University (NCTU), Hsinchu, Taiwan.

His research interest includes the design of microwave circuits.